Time-Domain Wavelet Galerkin Modeling of Two-Dimensional Electrically Large Dielectric Waveguides

Masafumi Fujii, *Member, IEEE,* and Wolfgang J. R. Hoefer, *Fellow, IEEE*

***Abstract*—The time-domain wavelet–Galerkin method based on Daubechies' compactly supported scaling functions of high regularity has been applied to the analysis of two-dimensional dielectric slab waveguides that have typical dimensions and material parameters of optical integrated waveguide components, and the results are compared with those obtained with the conventional finite-difference time-domain method. It has been found that the proposed method allows discretization with a much coarser grid than the conventional time-domain analysis techniques due to its local sampling and highly linear numerical dispersion properties. A series of numerical experiments demonstrates the capability of the method to simulate the wave propagation of electrically large inhomogeneous media with reduced computational expenditure.**

***Index Terms*—Daubechies wavelets, electromagnetic analysis, time-domain analysis, wavelet–Galerkin method.**

I. Introduction

RECENTLY, the wavelet–Galerkin scheme based on Daubechies' compactly supported scaling functions with two vanishing moments (D_2) was proposed by Cheong *et al.* [1]. The shifted interpolation property of Daubechies' wavelets adopted in Cheong's method enables local sampling of the field, leading to a versatile and simple algorithm for inhomogeneous media. Being a single-channel approach where only one-level scaling function is used as a basis function, unlike the conventional wavelet-based methods, such as the scaling-function-based multiresolution time-domain method (S-MRTD) [2], Cheong's method does not require computation of the constitutive relations of Maxwell's equations in spite of the large support and the asymmetry of the basis function.

The authors have extended the method by using Daubechies' scaling functions with three and four vanishing wavelet moments (denoted as D_3 and D_4, respectively) and investigated their fundamental numerical dispersion properties [3]. With basis functions of higher regularity, better accuracy is obtained. Moreover, by virtue of the minimum support of Daubechies' wavelets and scaling functions, the stencil size or the number of coefficients in the update equations is kept to a minimum, resulting in an optimally efficient algorithm.

The present algorithm is suitable for electrically large structures containing inhomogeneous media. One of the most interesting applications is the analysis of integrated planar optical waveguide components, which is computationally too expensive to solve with the conventional space-discrete methods such as the finite-difference time-domain (FDTD) method [4] and the transmission-line matrix (TLM) method [5] because the discretization must be small enough for these methods due to the numerical errors. In contrast to the beam propagation methods (BPMs) [6], [7], which are the most commonly used methods for analyzing optical waveguide components, the proposed method has the advantage as in FDTD [8] that it solves Maxwell's equations with only wavelet-expansion or finite-difference approximations, hence, reflection and radiation are inherently taken into account.

This paper addresses the two-dimensional time-domain wavelet–Galerkin method for TE polarization. In order to evaluate the accuracy and efficiency of the time-domain wavelet–Galerkin method, we demonstrate the analysis of two-dimensional dielectric slab waveguides including step and Y-shaped junction structures. The results are compared with those obtained with the conventional FDTD method. For open boundary conditions, the anisotropic uniaxial perfectly matched layer (UPML) [9] absorbing boundary condition (ABC) has been implemented; the performance of the UPML ABC is also evaluated to clarify its adaptability in the present scheme. The most important contribution of this paper is that, in the electrically large dielectric waveguides, convergence of the time-domain wavelet–Galerkin method and FDTD has been examined with different levels of discretization, and demonstrated a significant reduction of computational cost compared to FDTD; the proposed approach enables an accurate analysis of such waveguides with reflection and radiation taken into account that has been difficult to achieve with other numerical methods.

II. Formulation

Maxwell's equations for the two-dimensional TE polarization

$$-\mu\frac{\partial H_x}{\partial t} = -\frac{\partial E_y}{\partial z} \tag{1}$$

$$-\mu\frac{\partial H_z}{\partial t} = \frac{\partial E_y}{\partial x} \tag{2}$$

$$J_y + \sigma E_y + \epsilon\frac{\partial E_y}{\partial t} = \frac{\partial H_x}{\partial z} - \frac{\partial H_z}{\partial x} \tag{3}$$

are discretized on the standard Yee grid [4]. The basic formulation is also given in [3] and [10]. The field values are first ex-

Manuscript received February 10, 2000; revised August 1, 2000.

The authors are with the Department of Electrical and Computer Engineering, University of Victoria, Victoria, BC V8W 3P6, Canada (e-mail: fujii@engr.uvic.ca).

Publisher Item Identifier S 0018-9480(01)03299-9.

panded into the Daubechies' compactly supported scaling functions ϕ [11] as

$$E_y(x,z,t) = \sum_{i,k,n=-\infty}^{+\infty} E^{\phi}_{y,i,k,n-1/2}\phi_i(x)\phi_k(z)h_{n-1/2}(t) \tag{4}$$

$$H_x(x,z,t) = \sum_{i,k,n=-\infty}^{+\infty} H^{\phi}_{x,i,k+1/2,n}\phi_i(x)\phi_{k+1/2}(z)h_n(t) \tag{5}$$

$$H_z(x,z,t) = \sum_{i,k,n=-\infty}^{+\infty} H^{\phi}_{z,i+1/2,k,n}\phi_{i+1/2}(x)\phi_k(z)h_n(t) \tag{6}$$

where

$$h_n(t) = h\left(\frac{t}{\Delta t} - n + \frac{1}{2}\right) \tag{7}$$

is the well-known Haar scaling function [12] and

$$\phi_i(x) = \phi\left(\frac{x}{\Delta x} - i + M_1\right) \tag{8}$$

is the translated scaling function with $M_1 = \int_{-\infty}^{+\infty} x\phi(x)dx$ being the first-order moment of the scaling function.

The standard Galerkin's procedure leads to a system of time-evolution equations similar to the S-MRTD method [2] as

$$E^{\phi}_{y,i,k,n+1/2} = \frac{2\epsilon - \sigma\Delta t}{2\epsilon + \sigma\Delta t}E^{\phi}_{y,i,k,n-1/2} + \frac{2\Delta t}{2\epsilon + \sigma\Delta t} \cdot \left[\sum_{l=-L_s}^{L_s-1} a(l)\left(\frac{H^{\phi}_{x,i,k+l+1/2,n}}{\Delta z} - \frac{H^{\phi}_{z,i+l+1/2,k,n}}{\Delta x}\right) - J^{\phi}_{y,i,k,n}\right] \tag{9}$$

$$H^{\phi}_{x,i,k+1/2,n} = H^{\phi}_{x,i,k+1/2,n-1} + \frac{\Delta t}{\mu\Delta z}\sum_{l=-L_s}^{L_s-1} a(l)E^{\phi}_{y,i,k+l+1,n-1/2} \tag{10}$$

$$H^{\phi}_{z,i+1/2,k,n} = H^{\phi}_{z,i+1/2,k,n-1} + \frac{\Delta t}{\mu\Delta x}\sum_{l=-L_s}^{L_s-1} a(l)E^{\phi}_{y,i+l+1,k,n-1/2} \tag{11}$$

where L_s denotes the effective support of the basis function, i.e., the stencil size or the number of connection coefficients per side in the update equations. The coefficients connecting the scaling functions and their derivatives are listed in Table I

TABLE I
CONNECTION COEFFICIENTS $a(l)$, THE FIRST-ORDER MOMENTS M_1, AND THE STABILITY FACTOR s FOR D_2, D_3, AND D_4 SCALING FUNCTIONS

l	D_2	D_3	D_4
0	1.2291666667	1.2918129281	1.3110340773
1	-0.0937500000	-0.1371343465	-0.1560100710
2	0.0104166667	0.0287617723	0.0419957460
3		-0.0034701413	-0.0086543236
4		0.0000080265	0.0008308695
5			0.0000108999
6			-0.0000000041
M_1	0.6339743121	0.8174005815	1.0053923835
s	0.5303	0.4839	0.4657

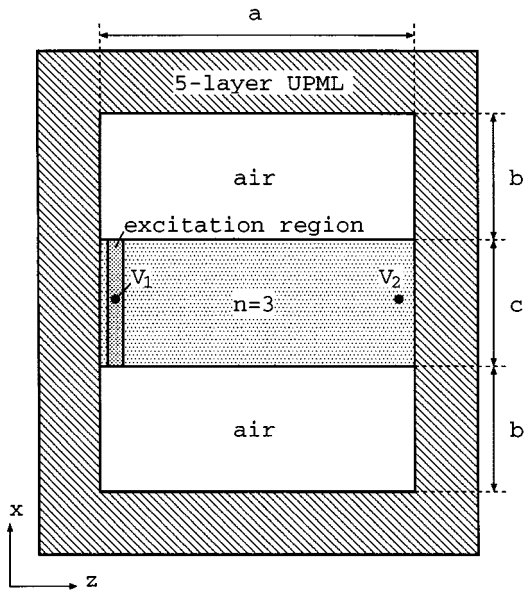

Fig. 1. Geometry of the straight optical waveguide. $a = 5\ \mu$m, $b = 2\ \mu$m, and $c = 2\ \mu$m.

[3], together with the first-order moments M_1 and the maximum limit of the stability factors for the two-dimensional square-grid case $s = 1/(\sqrt{2}\sum_l |a(l)|)$ [2]. The connection coefficients $a(l)$ for the negative argument can be obtained by $a(-l) = -a(l-1)$ for $l = 1, 2, \ldots$.

In order to truncate the analysis region, an UPML ABC [9] has been implemented. The UPML formulation in [9] yields the standard two-step updating procedure for the wavelet–Galerkin scheme. The first step is to update the electric flux density D_y from the magnetic field H_x and H_z

$$D^{\phi}_{y,i,k,n+1/2} = \frac{2\epsilon_0\kappa_z - \sigma_z\Delta t}{2\epsilon_0\kappa_z + \sigma_z\Delta t}D^{\phi}_{y,i,k,n-1/2} + \frac{2\epsilon_0\Delta t}{2\epsilon_0\kappa_z + \sigma_z\Delta t} \cdot \left[\sum_{l=-L_s}^{L_s-1} a(l)\left(\frac{H^{\phi}_{x,i,k+l+1/2,n}}{\Delta z} - \frac{H^{\phi}_{z,i+l+1/2,k,n}}{\Delta x}\right) - J^{\phi}_{y,i,k,n}\right]. \tag{12}$$

TABLE II
ANALYSIS CONDITIONS FOR THE STRAIGHT WAVEGUIDE. $N_{\max}$ IS THE NUMBER OF TIME STEPS. CPU TIME IS FOR USER PROCESS ONLY.

analysis scheme	grid type	Δx (μm)	Δz (μm)	number of Yee cells	N_{max}	memory Mbytes	CPU time
D_4	Coarse	0.1	0.1	70 × 60	5727	3	1 m 17 s
	Medium	0.1	0.05	70 × 110	9050	4	4 m 30 s
	Fine	0.05	0.025	130 × 210	18100	4.6	35 m 55 s
FDTD	Coarse	0.1	0.1	70 × 60	1168	3	19 s
	Medium	0.1	0.05	70 × 110	1846	4	46 s
	Fine	0.05	0.025	130 × 210	3693	4.6	4 m 9 s
	Extra-fine	0.025	0.0125	250 × 410	7387	8	20 m 57 s

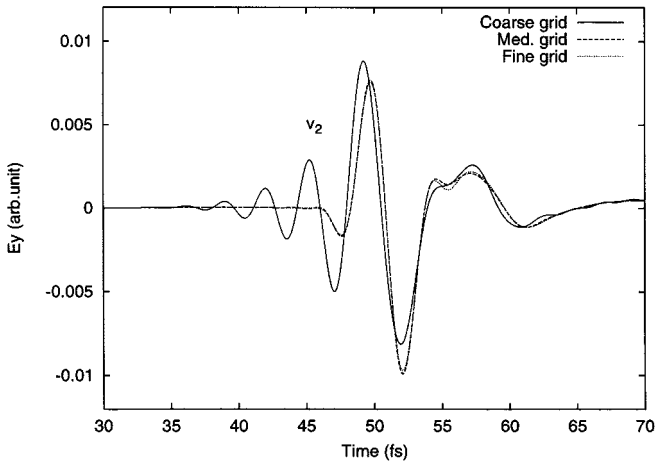

Fig. 2. Time data of the E_y-field in the straight optical waveguide detected at v_2 obtained with D_4 scaling function.

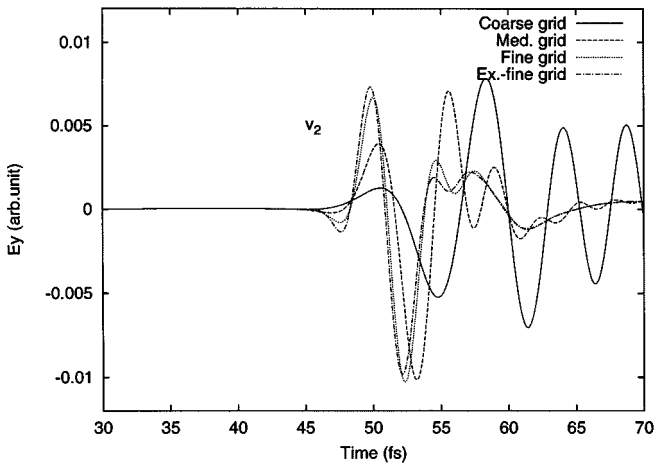

Fig. 3. Time data of the E_y-field in the straight optical waveguide detected at v_2 obtained with FDTD.

The second step is to update E_y from D_y locally without necessity to include the neighboring E_y or D_y due to the shifted interpolation property of the scaling functions

$$E^{\phi}_{y,i,k,n+1/2} = \frac{2\epsilon_0\kappa_x - \sigma_x\Delta t}{2\epsilon_0\kappa_x + \sigma_x\Delta t} E^{\phi}_{y,i,k,n-1/2} + \frac{2\epsilon_0\Delta t}{\epsilon_0\epsilon_r\left(2\epsilon_0\kappa_x + \sigma_x\Delta t\right)} \cdot \left[\left(\frac{\kappa_y}{\Delta t} + \frac{\sigma_y}{2\epsilon_0}\right) D^{\phi}_{y,i,k,n+1/2} - \left(\frac{\kappa_y}{\Delta t} - \frac{\sigma_y}{2\epsilon_0}\right) D^{\phi}_{y,i,k,n-1/2}\right]. \quad (13)$$

The update equations for the magnetic flux density B_x, B_z and the magnetic field H_x, H_z are obtained similarly.

As discussed in [9], these time-evolution equations can cover the whole analysis region simply by changing the material parameters for the inner computational region and the UPML region. The UPML material parameters are chosen to be $\sigma_\xi|_{\xi=x,z} = 0$ for the inner computational region, and $\sigma_\xi|_{\xi=x,z} > 0$ with fourth-order polynomial scaling $(m = 4)$ for the UPML region; the maximum value of σ at the end of the UPML region is chosen to be $\sigma_{\max} = (m+1)/(150\pi\Delta)$ [9], where Δ is the cell size either Δ_x or Δ_z perpendicular to the UPML interface with the regular region. The other parameter $\kappa_\xi|_{\xi=x,z} = 1$ over the whole region.

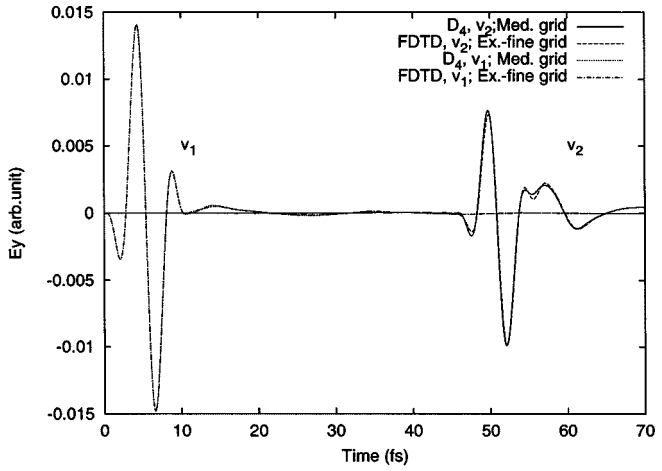

Fig. 4. Time data of the E_y-field in the straight optical waveguide detected at v_1 and v_2 compared for D_4 and FDTD with different grid sizes.

The UPML region is backed by a perfect electric conductor (PEC) wall implemented using the mirror principle. Although the basis functions are asymmetric, they satisfy the interpolation property and, thus, the mirror image is accurate at integer points. The basis functions have nonzero asymmetric values at noninteger points; nevertheless, this does not affect the numerical procedure.

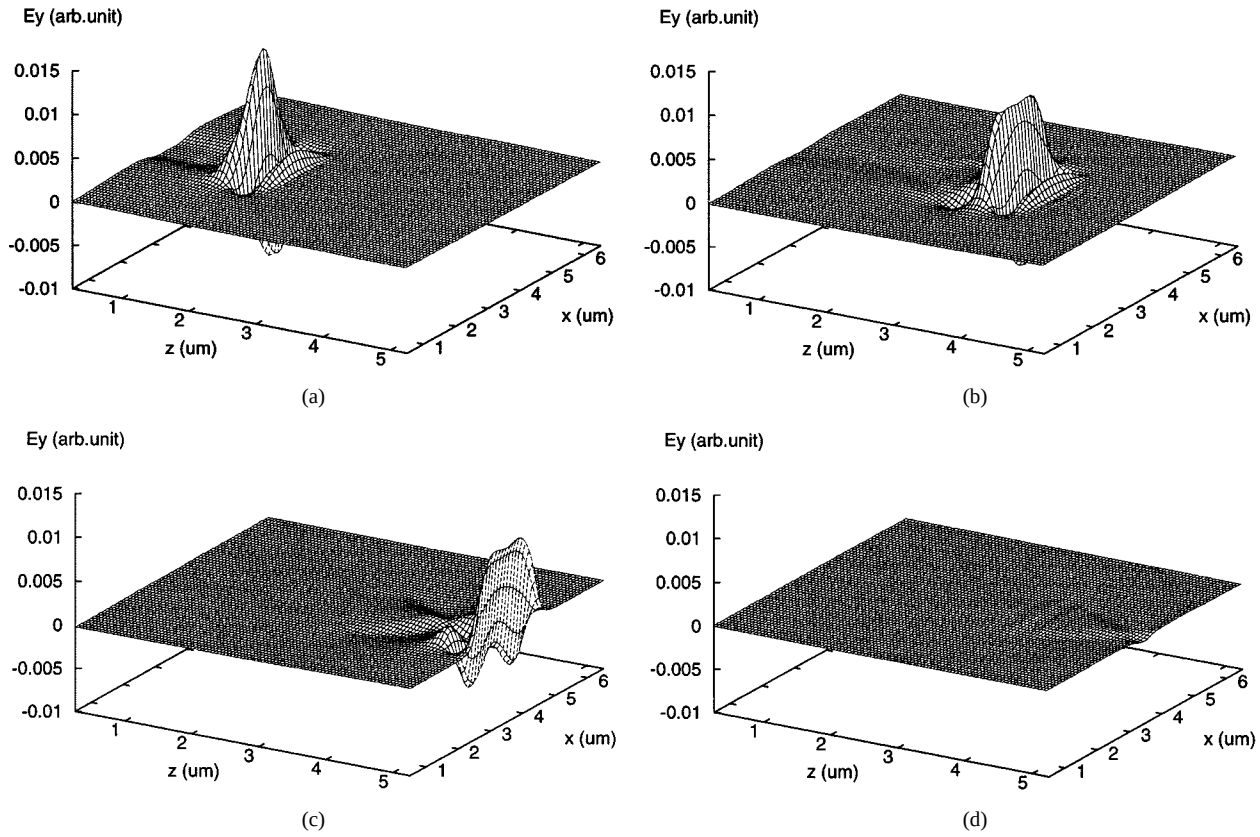

Fig. 5. Snapshots of the E_y-field in the straight optical waveguide. (a) 18 fs. (b) 36 fs. (c) 54 fs. (d) 72 fs.

III. Analysis of Dielectric Slab Waveguide Structures

A. Straight Waveguide

The TE-mode wave propagation in a straight optical waveguide was analyzed both with the D_4-based scheme and FDTD. Fig. 1 shows the geometry of the waveguide.

Convergence was examined with different discretizations for the D_4-based scheme and for FDTD. The analysis conditions are summarized in Table II. A raised-cosine modulated sine pulse with a single oscillation period was launched at the left-hand-side end of the waveguide. The spatial distribution of the excitation pulse was chosen to be similar to that of the fundamental propagation mode. The center frequency of the excitation pulse was about 193 THz, which corresponded to 1.55-μm wavelength in free space. The center dielectric slab had a refractive index $n = 3$ and was bounded by air regions, thus, the cell size was approximately 1/5–1/10 of the propagation wavelength. The source current had a raised-cosine distribution within the excitation region. The entire analysis region was surrounded by five layers of the UPML ABCs [9], which yielded less than 0.5% of reflection in this case, as discussed in the following section.

Figs. 2–4 show the time series signals of the E_y field detected at 0.2 μm from the UPML boundaries on the horizontal center of the waveguide (see v_1 and v_2 in Fig. 1). The distance between the two points is 4.6 μm. Figs. 2 and 3 are the E_y-field detected at v_2 for D_4 and FDTD, respectively. The results of the D_4-based scheme in Fig. 2 show good convergence for a medium grid, while those of FDTD in Fig. 3 show that convergence is still not observed even for a fine grid. The results of the D_4-based scheme with a medium grid and those of FDTD with an extra-fine grid are compared in Fig. 4, and they agree well. In comparison of the CPU time, the D_4-based scheme with a medium grid takes 4 min 30 s, while FDTD with an extra-fine grid takes 20 min 57 s. From these results, one can conclude that the D_4-based scheme has an advantage over FDTD in terms of both CPU time and memory requirement for the modeling of electrically large dielectric waveguides.

For the case of the D_4-based scheme with a medium grid, Fig. 5 demonstrates the snapshots of the wave propagation in the waveguide at every 18 fs from the start of the simulation.

B. Evaluation of the UPML ABC

The performance of the UPML ABC was evaluated for the particular case of the dielectric waveguide analyzed in this paper. The waveguide configuration for this test was the same as in Fig. 1, except for the shorter waveguide length $a = 1$ μm. The same excitation was launched in front of the interface of the regular and UPML regions, and time signals were detected at 0.2 μm in front of the other interface. To obtain a reflection-free reference signal, a 5-μm-long waveguide having the same geometry terminated with the same UPML ABC was used, and the computation was terminated before the reflected wave from the other side of the ABC reached the detector. Therefore, this experiment measures the reflection from the single interface in the direction of wave propagation. In this configuration, preliminary experiments have shown that sidewall effects are negligible.

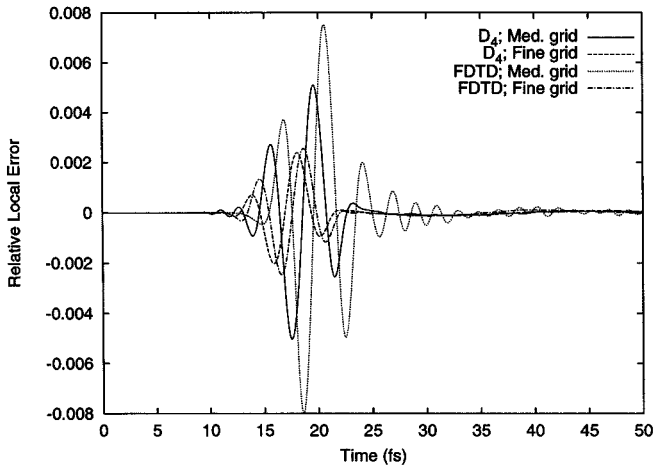

Fig. 6. Relative local error $[v(t) - v_0(t)]/[v_0(t)]_{\max}$ of the time signal reflected from the five-layer UPML.

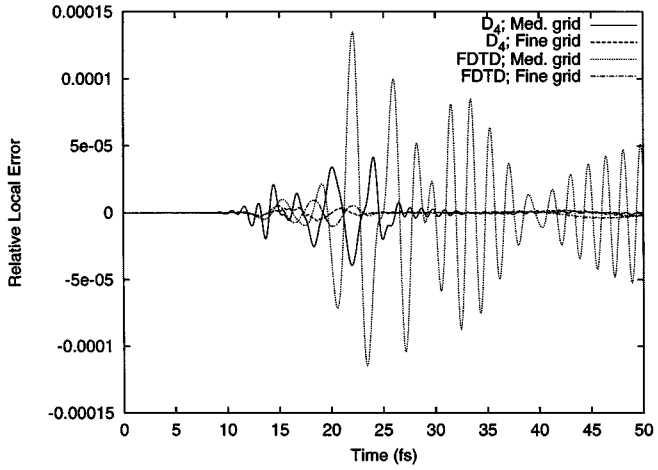

Fig. 7. Relative local error of the time signal reflected from the ten-layer UPML.

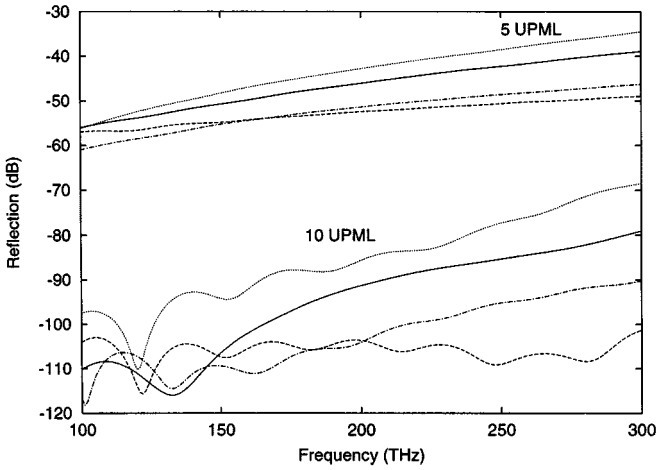

Fig. 8. Frequency spectra of the reflection coefficients of the five- and ten-layer UPML. —: D_4 medium grid, - - -: D_4 fine grid, $\cdots\cdots$: FDTD medium grid, and - · - · -: FDTD fine grid.

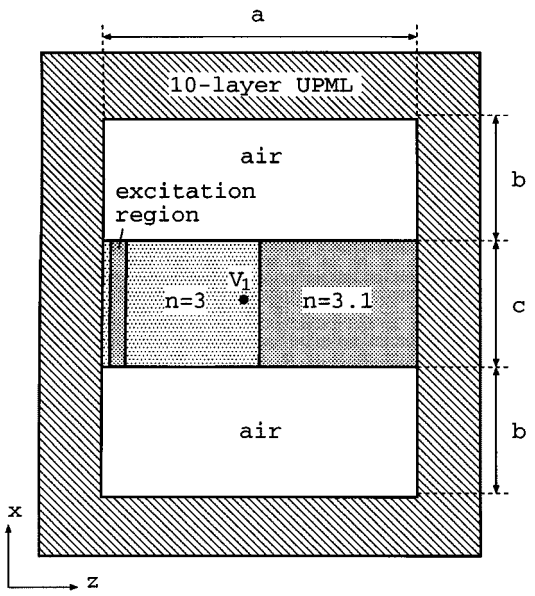

Fig. 9. Geometrical configuration of the step junction in the waveguide. $a = 5\ \mu$m, $b = 2\ \mu$m, and $c = 2\ \mu$m.

ABCs with five and ten layers were examined. Figs. 6 and 7 show the relative local reflection errors with respect to the maximum amplitude of the reference signal $v_0(t)$, namely, $[v(t) - v_0(t)]/[v_0(t)]_{\max}$, and Fig. 8 shows the reflection coefficients in frequency domain $\mathcal{F}[v(t) - v_0(t)]/\mathcal{F}[v_0(t)]$, where $\mathcal{F}[v(t)]$ denotes the Fourier transform of $v(t)$. These results show that, for the same discretization, the performance of the UPML is slightly better in the wavelet–Galerkin scheme than in FDTD because of the high linearity of the numerical dispersion of the wavelet–Galerkin scheme.

An important observation of these results is that the performance of the UPML–ABC is more sensitive to the number of PML layers than the grid size; even if the grid size increases slightly, a desired level of absorption can be maintained by using the similar number of the PML layers.

C. Step Junction

The reflection from a step in the dielectric constant of the same waveguide shown in Fig. 9 has also been analyzed. In order to detect the small reflected signal, an UPML ABC with ten layers has been employed; the reflection from the ABC is expected to be less than -80 dB. As in the previous sections, coarse to extra-fine grids are used in the analysis.

The frequency spectra of the reflection from the step junction is shown in Fig. 10. The results obtained with a coarse grid are not shown because they have large errors due to the large numerical dispersion. The results of the D_4-based scheme are in line with those from FDTD with extra-fine grid because of the highly linear numerical dispersion of the scheme, while FDTD with medium and fine grids yields erroneous values. The deviation in the amplitude of the reflection is mainly due to the error in the modeling of the location of dielectric material boundaries that is inherent to any space-discrete methods. This error will be suppressed by adding wavelet terms in the region of material boundaries without seriously increasing the computational overhead, which will be the subject of future research.

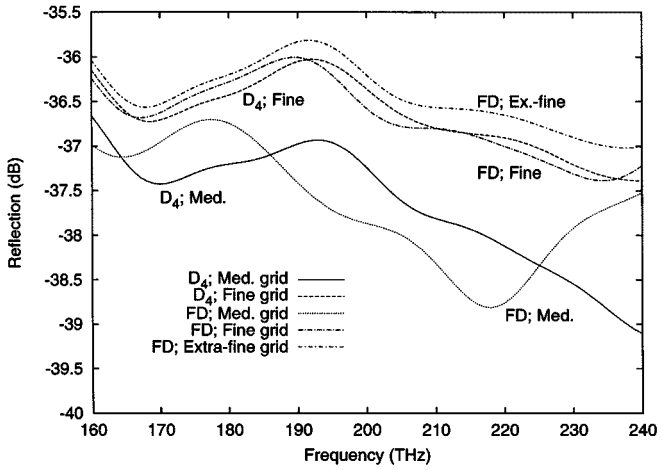

Fig. 10. Frequency spectra of the reflection coefficient of the step junction.

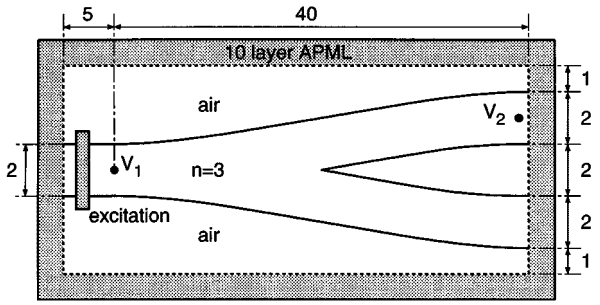

Fig. 11. Two-dimensional Y-shaped junction under test. Unit is micrometers.

D. Y-Shaped Junction

A Y-shaped junction structure was analyzed with the D_4-based scheme to evaluate the adaptability of the proposed method to optical waveguides of practical engineering interest in the two-dimensional case. This will give further insight into the method when it is extended to the three-dimensional case.

The Y-shaped junction shown in Fig. 11 is a simplified two-dimensional version of the original three-dimensional counterpart that has been already analyzed with various BPMs [6], [7]. The dielectric slab in our case has a refractive index $n = 3$ and is bounded by air. The initial 5-μm-long and 2-μm-wide waveguide section branches into two identical waveguides while maintaining the same width, and the center of the waveguide traces $x(z) = \pm[1 - \cos(\pi z/L)]$, where the length of the junction section is $L = 40$ μm. The curvature of the slab–air boundary was modeled using a staircase approximation. The entire analysis region 45 μm $\times$ 8 μm is surrounded by ten-layer UPML ABCs.

The structure was analyzed with two different discretizations: medium ($\Delta x = 0.1$ μm, $\Delta z = 0.05$ μm), and medium-fine ($\Delta x = 0.05$ μm, $\Delta z = 0.05$ μm); the number of Yee cells is 100 $\times$ 920 for the medium grid and 180 $\times$ 920 for the medium-fine grid including the UPML. The time duration of the analysis was 2 ps, the time step Δt was chosen to be 0.2 times the maximum Courant limit of the corresponding FDTD method, and the number of time steps was 201 111 for the medium grid and 254 388 for the medium-fine grid. The time signal was detected at 5 μm from the left-hand-side end (v_1) and at 0.2 μm from the right-hand-side end (v_2) of the waveguide.

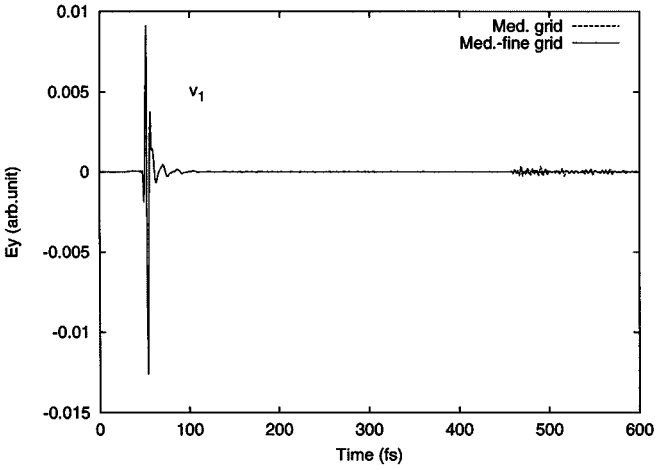

Fig. 12. Time series data of the Y-shaped junction structure obtained with the D_4-based scheme. The incident and reflected signals at v_1 are shown.

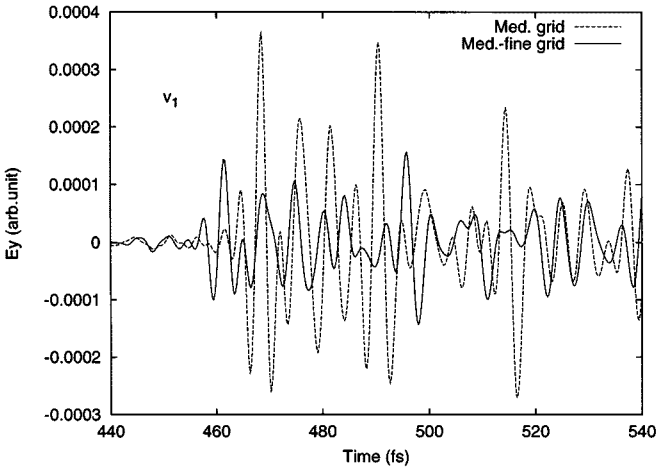

Fig. 13. Time series data of the Y-shaped junction structure obtained with the D_4-based scheme. The reflected signal at v_1 is shown.

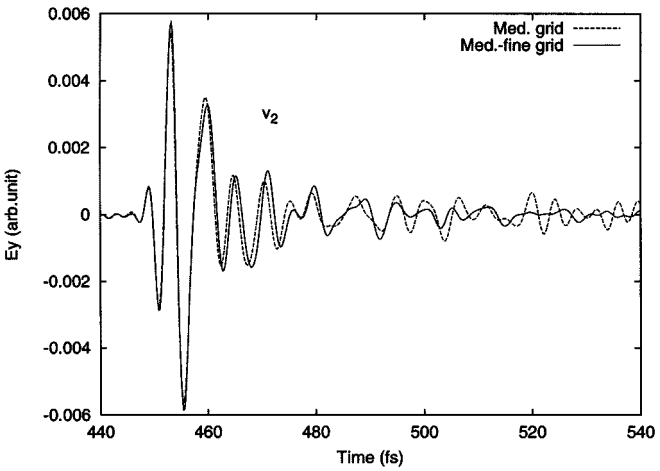

Fig. 14. Time series data of the Y-shaped junction structure obtained with the D_4-based scheme. The transmitted signal at v_2 is shown.

The user-process CPU time was 14 h for the medium grid and 32 h for the medium-fine grid with a Sun Ultra workstation of 270-MHz clock rate and 256-MB memory. The executable file size was about 20 MB for the medium-fine grid.

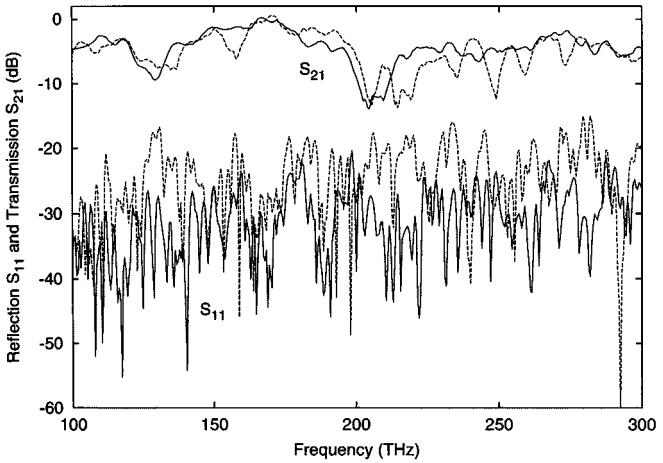

Fig. 15. Frequency spectra of the reflection (S_{11}) and transmission (S_{21}) of the Y-shaped junction obtained with the D_4-based scheme, - - -: medium grid, —: medium-fine grid.

The resulting time data are compared in Figs. 12–14. Due to the staircase approximation, the reflection from the junction section is smaller for the medium-fine grid than for the medium grid. The transmitted signals agree better in the wavefront than in the tail for both discretizations. This can be due also to the discretization error in the x-direction for the medium grid. The frequency-domain data in Figs. 15 show that the reflection from the junction is about -20 to -30 dB.

IV. Conclusion

The time-domain wavelet–Galerkin method based on Daubechies' compactly supported scaling functions with three and four vanishing moments has been applied to the analysis of two-dimensional electrically large dielectric waveguides having a typical dimension of optical waveguide components.

The minimum support property of Daubechies' scaling functions yields effective algorithm, and the highly linear numerical dispersion property of the analysis method reduces the number of cells in the analysis, thus enabling the solution of the time-dependent Maxwell's equations for electrically large inhomogeneous structures with a reduced computational effort compared to the conventional FDTD method.

Sample waveguides were analyzed with different discretization levels, and good convergence was indeed obtained with the wavelet–Galerkin method, while with FDTD, much finer grids were needed for sufficient convergence.

It will be straightforward to extend this method to the three-dimensional case, leading potentially to a full-wave solution of such waveguides that could not be solved with the FDTD method due to excessive computational requirements.

References

[1] Y. W. Cheong, Y. M. Lee, K. H. Ra, J. G. Kang, and C. C. Shin, "Wavelet–Galerkin scheme of time-dependent inhomogeneous electromagnetic problems," *IEEE Microwave Guided Wave Lett.*, vol. 9, pp. 297–299, Aug. 1999.

[2] M. Krumpholz and L. P. B. Katehi, "MRTD: New time-domain schemes based on multiresolution analysis," *IEEE Trans. Microwave Theory Tech.*, vol. 44, pp. 555–571, Apr. 1996.

[3] M. Fujii and W. J. R. Hoefer, "Dispersion of time domain wavelet–Galerkin method based on Daubechies' compactly supported scaling functions with three and four vanishing moments," *IEEE Microwave Guided Wave Lett.*, vol. 10, pp. 125–127, Apr. 2000.

[4] K. S. Yee, "Numerical solution of initial boundary value problems involving Maxwell's equation in isotropic media," *IEEE Trans. Antennas Propagat.*, vol. 14, pp. 302–307, May 1966.

[5] W. J. R. Hoefer, "The transmission-line matrix method—Theory and applications," *IEEE Trans. Microwave Theory Tech.*, vol. MTT-33, pp. 882–893, Oct. 1985.

[6] P.-C. Lee and E. Voges, "Three-dimensional semi-vectorial wide-angle beam propagation method," *J. Lightwave Technol.*, vol. 12, pp. 215–225, Feb. 1994.

[7] Y. Tsuji, M. Koshiba, and T. Shiraishi, "Finite element beam propagation method for three-dimensional optical waveguide structures," *J. Lightwave Technol.*, vol. 15, pp. 1728–1734, Sept. 1997.

[8] S. T. Chu and S. K. Chaudhuri, "Combining modal analysis and the finite-difference time-domain method in the study of dielectric waveguide problems," *IEEE Trans. Microwave Theory Tech.*, vol. 38, pp. 1755–1760, Nov. 1990.

[9] S. D. Gedney, "An anisotropic perfectly matched layer absorbing media for the truncation of FDTD lattices," *IEEE Trans. Antennas Propagat.*, vol. 44, pp. 1630–1639, Dec. 1996.

[10] M. Fujii and W. J. R. Hoefer, "Application of wavelet–Galerkin method to electrically-large optical waveguide problems," in *IEEE MTT-S Int. Microwave Symp. Dig.*, 2000, paper TU3E–3.

[11] I. Daubechies, *Ten Lectures on Wavelets*. Philadelphia, PA: SIAM, 1992.

[12] M. Fujii and W. J. R. Hoefer, "A three-dimensional Haar-wavelet-based multiresolution analysis similar to the FDTD method—Derivation and application," *IEEE Trans. Microwave Theory Tech.*, vol. 46, pp. 2463–2475, Dec. 1998.

Masafumi Fujii (S'97–M'99) was born in Osaka, Japan, in 1966. He received the B.E. and M.E. degrees in electrical and electronic engineering from Kobe University, Kobe, Japan, in 1989 and 1991, respectively, and the Ph.D. degree from the University of Victoria, Victoria, BC, Canada, in 1999.

From 1991 to 1998, he was with the Sumitomo Metal Industries Ltd., Osaka, Japan, where he was involved in numerical analysis and measurement of microwave components. He is currently a Post-Doctoral Research Fellow in the Department of Electrical and Computer Engineering, University of Victoria. His research interest is in the area of numerical analysis and modeling of electromagnetic fields using wavelets.

Wolfgang J. R. Hoefer (M'71–SM'78–F'91) received the Dipl.-Ing. degree in electrical engineering from the Technische Hochschule Aachen, Aachen, Germany, in 1965, and the D.Ing. degree from the Universitaire de Technologie de Grenoble, Grenoble, France, in 1968.

From 1968 to 1969, he was a Lecturer at the Institut Universitaire de Technologie de Grenoble, Grenoble, France, and a Research Fellow at the Institut National Polytechnique de Grenoble, Grenoble, France. In 1969, he joined the Department of Electrical Engineering, University of Ottawa, Ottawa, ON, Canada, where he was a Professor until March 1992. Since April 1992, he has held the NSERC/MPR Teltech Industrial Research Chair in RF Engineering, Department of Electrical and Computer Engineering, University of Victoria, Victoria, BC, Canada, and is a Fellow of the Advanced Systems Institute of British Columbia. During sabbatical leaves in 1976 and 1977, he spent six months with the Space Division of AEG-Telefunken (now ATN), Backnang, Germany, and six months with the Electromagnetics Laboratory, Institut National Polytechnique de Grenoble. From 1984 to 1985, he was a Visiting Scientist at the Space Electronics Directorate, Communications Research Center, Ottawa, ON, Canada. From 1990 to 1991, he spent a third sabbatical year as a Visiting Professor at the Universities of Rome Tor Vergata, Rome, Italy, Nice-Sophia Antipolis, Nice-Sophia, France, and TUM, Munich, Germany. His research interests include numerical techniques for modeling electromagnetic fields and waves, computer-aided design (CAD) of microwave and millimeter-wave circuits, microwave measurement techniques, and engineering education. He is the co-founder and Managing Editor of the *International Journal of Numerical Modeling*.

Dr. Hoefer is Chair of the IEEE Microwave Theory and Techniques Society (IEEE MTT-S) MTT-15 Technical Committee on Microwave Field Theory. He was an associate editor for the IEEE TRANSACTIONS ON MICROWAVE THEORY AND TECHNIQUES.